frontiers in Physics

BRIEF RESEARCH REPORT
published: 15 December 2021
doi: 10.3389/fphy.2021.783136

Structural Stability of Pyrochlore Manganate $In_2Mn_2O_7$ Under High Pressure

Hui Li[1,2], *Shuailing Ma*[1]*, *Jili Ye*[2] *and Xin Wang*[1]*

[1]State Key Laboratory of Superhard Materials, College of Physics, Jilin University, Changchun, China, [2]School of Mathematics and Physics, Key Laboratory for Ionospheric Observation and Simulation, Guangxi University for Nationalities, Nanning, China

The pyrochlore manganate $In_2Mn_2O_7$ is a very promising ferromagnetic semiconductor material, which has a good application prospect in spin transport due to its very low electron effective mass, high Curie temperature, and structural stability. In this paper, $In_2Mn_2O_7$ with pyrochlore structure was successfully prepared by high temperature and high pressure combined with the sol–gel method, and the *in situ* high-pressure X-ray diffraction experiment was carried out on it. The results showed that the structure of $In_2Mn_2O_7$ was very stable in the pressure range of 0–29.0 GPa, and its bulk modulus was given. This lays a foundation for the application of $In_2Mn_2O_7$ in extreme environments.

Keywords: pyrochlore, manganate, high pressure, high temperature, structural stability

OPEN ACCESS

Edited by:
Ralph Ernstorfer,
Technical University of Berlin, Germany

Reviewed by:
Surajit Chatterjee,
University of Michigan, United States
Hiroshi Fukui,
Japan Synchrotron Radiation Research Institute, Japan

***Correspondence:**
Shuailing Ma
msljlu@163.com
Xin Wang
xin_wang@jlu.edu.cn

Specialty section:
This article was submitted to Physical Chemistry and Chemical Physics, a section of the journal Frontiers in Physics

Received: *25 September 2021*
Accepted: *17 November 2021*
Published: *15 December 2021*

Citation:
Li H, Ma S, Ye J and Wang X (2021) Structural Stability of Pyrochlore Manganate $In_2Mn_2O_7$ Under High Pressure. Front. Phys. 9:783136. doi: 10.3389/fphy.2021.783136

INTRODUCTION

In the past decades, there has been increasing interest in the pyrochlore oxide materials (general formula $A_2B_2O_7$) for the studies in both basic science [1, 2] and engineering [3]. Due to the tetrahedral geometry of cations in pyrochlore, very rich quantum phenomena were discovered recently. For example, $Ho_2Ti_2O_7$ and $Dy_2Ti_2O_7$ are Ising pyrochlore materials with Ising anisotropy and effective antiferromagnetic exchange interaction [4]. They have classical spin-ice ground state, and the magnetic moment at each tetrahedral vertex forms a two-in and a two-out degenerate distribution. Besides, the anomalous Hall effect is found in $Nd_2Mo_2O_7$ [5], the giant magnetoresistance in $Ti_2Mn_2O_7$ [6], and the topological state in $A_2Ir_2O_7$ [7].

Materials combining semiconductivity and magnetism open up possibilities for novel electronic devices that utilize electron spin in addition to charge degrees of freedom [8, 9]. The ferromagnetic semiconductor has attracted special attention because of its spin polarization transport potential in spintronics. A closely related important technical phenomenon is spin filtering, which can be achieved by using ferromagnetic semiconductors as tunneling barriers to generate high spin polarization currents [10, 11]. Ferromagnetic semiconductors used in spintronics are mainly based on magnetic impurities embedded in conventional non-magnetic semiconductors [12]. The robustness of carrier-induced ferromagnetism is very sensitive to the growth conditions and processing methods. The origin of room-temperature ferromagnetism of doped magnetic semiconductors is still a controversial topic. In contrast, undoped magnetic semiconductors exhibit long-range magnetism independent of external doping. At present, some undoped ferromagnetic semiconductors have been reported, mainly including halide $CrBr_3$ [13], CrI_3 [14–16], Mn-based pyrochlore oxide [17], perovskite oxide $BiMnO_3$ [18], $CuSeO_3$ [19], and $YTiO_3$ [20]. The ferromagnetic semiconductor most studied in spintronics is europium chalcogenide compound EuX (X = O, S, Se) [10, 21–24]. EuX has good performance in spin filter devices, but the Curie temperature is very low [e.g., Tc(EuO) = 69 K [25]], which is a characteristic of most ferromagnetic semiconductors currently known. In addition, the electronic structure of ferromagnetic

semiconductors needs to be adjusted in the context of spin transport. The electron injection efficiency is determined by the exchange splitting of the conduction band, and low electron effective mass is the key to achieve high carrier mobility. Similarly, exchange splitting is also important for spin filtering because it produces spin-dependent tunneling current barriers.

Therefore, the combination of strong ferromagnetism and attractive semiconductor properties in a material is ideal, but it is still an issue that needs further study. Wei Chen et al. searched for undoped ferromagnetic semiconductors through high-throughput computational screening [26]. They found that magnetic pyrochlore oxide $In_2Mn_2O_7$ has a good application prospect in spin transport due to its very low effective electron mass, large exchange splitting of conduction band, stability in air, and high Curie temperature of 130 K. Therefore, the study of the structural stability of $In_2Mn_2O_7$ under high pressure is of great significance for the application of it under extreme conditions. In this paper, we have successfully synthesized pyrochlore $In_2Mn_2O_7$. The structural stability $In_2Mn_2O_7$ has been investigated by angle-dispersive synchrotron X-ray powder diffraction at high pressures.

EXPERIMENT

Sample Preparation

In this experiment, $In_2Mn_2O_7$ was synthesized by the sol–gel method combined with the high-temperature and high-pressure (HTHP) method. In_2O_3 (99.99% purity), MnO (99.9% purity), citric acid (AR: analytical reagent), and nitric acid (AR) were used as raw materials. In_2O_3 and MnO with the molar ratio of 1:2 were dissolved in nitric acid and diluted in distilled water. Citric acid was then added as a fuel to the above solution to yield a citrate/nitrate ratio of 1.2. The mixed solution was continuously stirred using a magnetic agitator. The solution was evaporated by heating at 150°C until a brown sticky gel was formed. Subsequently, the gel was dried at a temperature up to 200°C. The dried gel was calcined at 500°C in air for 10 h.

Next, the target product was synthesized by the cubic anvil HPHT apparatus. The powder was pressed into cylindrical samples with a diameter of 6 mm and a height of 2.3 mm. The cylindrical sample was put into the sample synthesis chamber with a specific combination, and the chamber was put into the cubic anvil HPHT apparatus (SPD6×600) [27, 28]. The temperature was raised to 1,300°C, and the pressure was increased to 5 GPa. The heat and pressure preservation time was 60 min. At last, we made the temperature drop rapidly to room temperature within 15 s, and the pressure needed to be reduced slowly to obtain pyrochlore $In_2Mn_2O_7$.

X-Ray Diffractometry

In the ambient condition, the phase purity was detected by powder X-ray diffraction (XRD) measurements using a Rigaku Rotaflex X-ray diffractometer with Cu-Kα radiation (λ = 1.54056Å) at room temperature. The test voltage was 40 kV, the current was 30 mA, the scanning range was 10–90°, and the scanning speed was 4°/min. The high-pressure angle-dispersive XRD patterns were collected at the beamline X17C of the National Synchrotron Light Source at Brookhaven for $In_2Mn_2O_7$ with a monochromic wavelength of 0.4112 Å. A diamond anvil cell (DAC) with an anvil culet of 300 μm diameter was utilized to generate high pressure with the T301 stainless steel as the gasket, which was pre-indented to a 50 μm thickness. One piece of the as-prepared samples, a small piece of ruby as the pressure calibrant [29], and a 16:3:1 methanol/ethanol/water mixture as the pressure-transmitting medium were loaded into the diamond anvil cells. The distance between the sample and the detector and parameters of the detector were calibrated using a CeO_2 standard. All the diffraction data were collected using an MAR CCD detector, and the diffraction profiles were obtained *via* the radial integration of the two-dimensional diffraction rings using FIT2D software [30]. Rietveld analyses were performed with the software GSAS [31].

RESULTS AND ANALYSIS

XRD Analysis

The structure of $In_2Mn_2O_7$ was determined by Rietveld refinement, shown in **Figure 1A**. The red, blue, and black lines in the figure represent the experiment curve, the calculation curve, and the difference between them, respectively. The green vertical line represents the fitted peak position. From the fitted results, it was determined that the compound $In_2Mn_2O_7$ crystallized in the cubic system, with the space group *Fd-3m* (No. 227) and cell parameters a = 9.7113(5)Å, V = 915.8(6)$Å^3$, and Z = 8. $In_2Mn_2O_7$ can be formulated as $In_2Mn_2O_6O'$, with Mn ions at 16*c*, In ions at 16*d*, O at 48*f*, and O′ at 8*b*. In ions formed twisted cubes with surrounding oxygen atoms, and Mn ions formed twisted octahedrons with surrounding oxygen atoms. It was worth noting that there was only one adjustable position parameter in this structure, which was the *x* coordinate of the oxygen atom at the position of 48*f*. **Figure 1B** is the schematic diagram of its structure. The refinement parameters of the cubic phase $In_2Mn_2O_7$ structure are given in **Table 1**.

In Situ High-Pressure X-Ray Diffraction

The *in situ* XRD patterns of $In_2Mn_2O_7$ at various pressures up to 29.0 GPa have been collected, and a few representative patterns are shown in **Figure 2**. The results showed that, in the whole pressure range of this experiment, there was no obvious change in the high-pressure XRD diffraction pattern, and there appeared no new diffraction peak. The diffraction peak under each pressure point moved to a higher angle with increasing pressures, accompanied by the weakening of the intensity of diffraction peak, which was usually caused by the increase of lattice disorder under pressure. This indicated that the cell volume of $In_2Mn_2O_7$ decreased gradually in the test pressure range of 0–29.0 GPa. After releasing the pressure, the positions of diffraction peaks were almost the same as those before pressure rise. The above two points indicated that the cubic phase $In_2Mn_2O_7$ exhibited excellent structural stability in the whole pressure range in this experiment. When the pressure increased gradually, the compound had no structural phase transition but only slightly

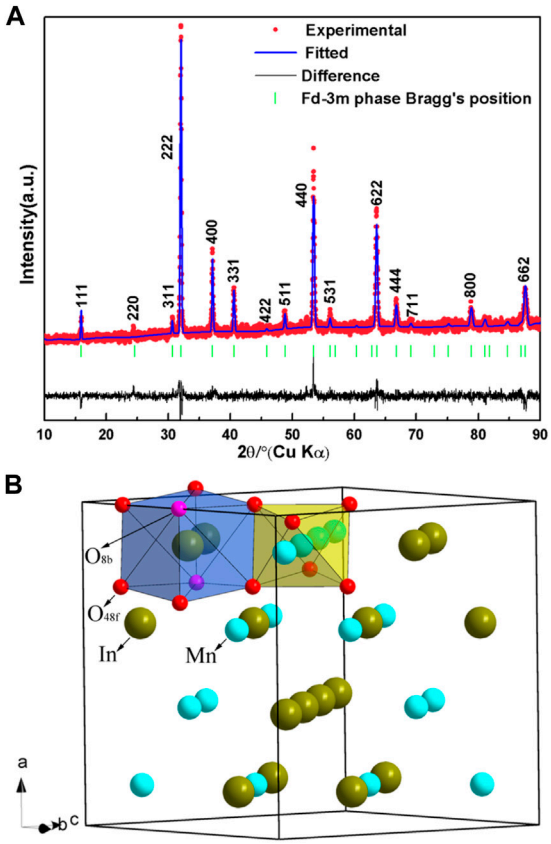

FIGURE 1 | (A) Rietveld full-profile refinement of the diffraction patterns of $In_2Mn_2O_7$ at ambient condition. Red, blue, and black solid lines represent experimental, calculated, and residual patterns, respectively. Vertical markers show the calculated peak positions. **(B)** A schematic representation of the crystal structures of pyrochlore-type $In_2Mn_2O_7$.

strained, and this change disappeared completely after the pressure was removed. In order to further study the change of the crystal structure of $In_2Mn_2O_7$ with pressure, Rietveld analyses were performed with the software GSAS under various pressures. We obtained the lattice constants given in **Table 1** and volumes under different pressures as shown in **Figure 3**.

The P–V data were fitted using the Birch–Murnaghan (B–M) equation of state [32], expressed as follows:

$$P = \frac{3.0}{2} B_o \left[\left(\frac{V_0}{V}\right)^{\frac{7}{3}} - \left(\frac{V_0}{V}\right)^{\frac{5}{3}} \right] \times \left\{ 1 + \frac{3}{4}\left(B'_o - 4\right) \times \left[\left(\frac{V_0}{V}\right)^{\frac{2}{3}} - 1 \right] \right\}, \quad (1)$$

where B_0 represents the bulk modulus at zero pressure, B'_o represents the first derivative of the bulk modulus, and V_0 represents the volume of a single cell at zero pressure. Taking $B'_o = 4$, the fitting results are shown as the red curve in **Figure 3**. It can be seen that the red curve fitted very well with the experimental data within the experimental pressure range, and the fitting results showed that $B_0 = 240(4)$ GPa. In addition, when B'_o was not fixed as 4, we obtained B = 221(6) GPa and B'_o = 5.5(1.2), shown with the fluorescent green dotted line in **Figure 3**.

TABLE 1 | Refined atomic coordinates of $In_2Mn_2O_7$ at ambient condition and lattice parameters at various pressures.

Atoms	***Wyckoff* (*x y z*)**
In	16d (0.5 0.5 0.5)
Mn	16c (0 0 0)
O(1)	48f [0.125 0.125 0. 0.3241(9)]
O(2)	8b (0.325 0.325 0.325)
Residuals[1] (%)	R_{wp}: 6.27%
	R_p: 5.08%
Pressure (GPa)	**Lattice parameter (Å)**
0.6	9.6983(7)
1.6	9.6786(4)
3.2	9.6474(3)
5.0	9.6296(2)
6.2	9.6087(7)
7.4	9.5892(2)
9.5	9.5707(1)
10.8	9.5579(2)
12.4	9.5390(3)
14.0	9.5268(6)
15.5	9.5102(1)
17.3	9.4937(2)
19.4	9.4788(4)
21.0	9.4517(5)
22.9	9.4368(5)
27.0	9.3993(3)
29.0	9.3764(2)

Note: [1]R_{wp} and R_p as defined in GSAS [29].

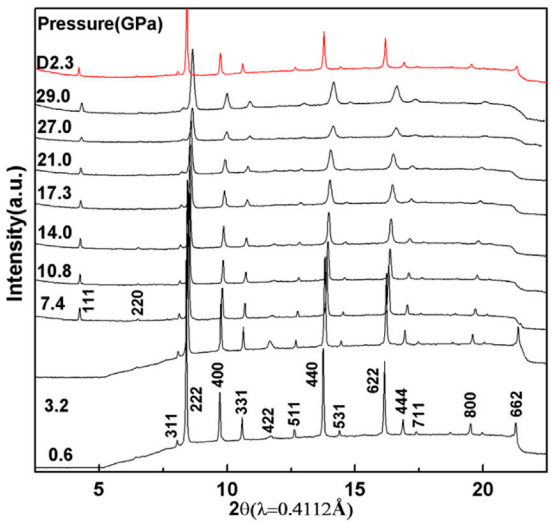

FIGURE 2 | Angle-dispersive XRD patterns of $In_2Mn_2O_7$ at selected pressures with a monochromic wavelength of 0.4112 Å at room temperature. The top red pattern was taken from the samples after the release of pressure.

This result was compared with the bulk moduli of other $A_2B_2O_7$ pyrochlore oxides. The bulk moduli of $A_2Ti_2O_7$ (A = Ho, Y, Tb, Sm) compounds were 213(2), 204(3), 199(1), and 164.8(1.5) GPa [33, 34], and the bulk moduli of $A_2Sn_2O_7$ (A = La, Eu) compounds were 180(6) and 170 GPa, respectively [35]. It can be seen that the bulk modulus of $In_2Mn_2O_7$ was obviously larger than that of the above compounds. However, we also studied

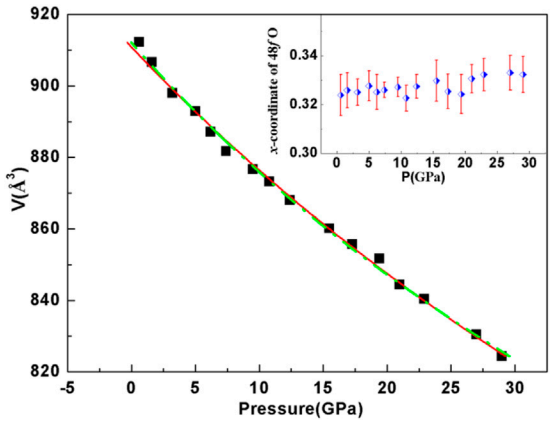

FIGURE 3 | Observed P–V variation fitted with the third-order Birch–Murnaghan (B–M) equation of state for $In_2Mn_2O_7$. Birch–Murnaghan EOS fits for the data are shown with the dotted line, B = 221(6) GPa, B'_o = 5.5(1.2), and solid line, B = 240(4) GPa, B'_o held at 4. The inset shows the pressure dependence of the x parameter for the O_{48f} atom.

$A_2Ge_2O_7$ (A = In, Ho, Sc) oxides before and obtained that their bulk moduli were 279(4), 328(7), and 263(4) GPa, respectively [36–38]. The bulk modulus is one of the most important physical parameters that characterize the mechanical property of materials. Several works have suggested that the bond length should be taken into account to explain the variation of the bulk modulus of materials [39, 40]. It has been known that the bulk modulus is proportional to k/d^n, where d is the bond length and k, n are determined by the properties of materials [40, 41]. Changes in the electronic configuration of the A and B atoms of $A_2B_2O_7$ pyrochlore oxides have an effect on the length of the bond. Ionic, covalent, and metallic bonds can affect bond strength which is closely related to the bond length. So to find the laws and the physical mechanisms behind these bulk moduli, further research is needed.

In the ordered cubic pyrochlore structure, all the atoms are in special positions except O_{48f}. Hence, the structure is entirely described by the *x* positional parameter of O_{48f}. The X-ray diffraction patterns were refined by the Rietveld method up to 29.0 GPa. The refined x parameter for O_{48f} as a function of pressure is shown in the inset of **Figure 3**. Previous studies on pyrochlore oxides have revealed that the sudden change of the *x* positional parameter of the O_{48f} atom existed in the process of pressure-induced structural phase transition. For example, with increasing pressure, the ordered pyrochlore $Gd_2Zr_2O_7$ begins to transform to a disordered defect-fluorite–type cubic structure up to 15 GPa. Above 15 GPa, a high-pressure phase forms that has a distorted defect-fluorite–type structure of lower symmetry. Below 10 GPa, there is no or little change in the refined x parameter for O_{48f}, followed by a rapid decrease with increasing pressure [42]. Above 18 GPa, the pyrochlore $Sm_2Zr_2O_7$ is unstable, and a pressure-induced phase transition occurred. The x coordinate for the 48f oxygen increases dramatically after 16 GPa [43]. Within the range of our study, it can be seen that x_{O48f} has no sudden change, which also indicates the structural stability of pyrochlore $In_2Mn_2O_7$.

CONCLUSION

In this paper, the manganate $In_2Mn_2O_7$ was successfully prepared by the sol–gel method combined with high temperature and high pressure. Through XRD characterization at atmospheric pressure, $In_2Mn_2O_7$ was identified as a pyrochlore structure, and its exact crystallographic data and structural refinement parameters were given. Through *in situ* high-pressure X-ray diffraction, it was found that $In_2Mn_2O_7$ had no structural phase transition below 29.0 GPa, showing excellent structural stability. By fitting the P–V curve with the Birch–Murnaghan (B–M) equation of state, the bulk modulus of the sample was obtained as 240(4) GPa. This lays a foundation for the application of $In_2Mn_2O_7$ in extreme environments.

DATA AVAILABILITY STATEMENT

The original contributions presented in the study are included in the article/supplementary material, and further inquiries can be directed to the corresponding authors.

AUTHOR CONTRIBUTIONS

XW contributed to the conception and design of the study and completed the high-pressure part of the experiment. HL completed sample synthesis. HL and SM performed the design of figures and wrote the first draft of the manuscript. JY organized the literature. All authors contributed to manuscript revision and read and approved the submitted version.

FUNDING

This research was supported by the Guangxi Natural Science Foundation under Grant Nos. 2018GXNSFBA050034 and 2019GXNSFBA185001, the Open Project of State Key Laboratory of Superhard Materials (Jilin University) (202107), and the Young and Middle-aged Teachers' Basic Ability Improvement Project of Guangxi Department of Education (No. 2020KY04023).

ACKNOWLEDGMENTS

We acknowledge Zhiqiang Chen and Xinguo Hong for technical support with the high-pressure experiments at the X17C beamline of the NSLS.

REFERENCES

1. Gardner JS, Gingras M, Greedan JE. Magnetic Pyrochlore Oxides[J]. *Rev Mod Phys* (2010) 82(1). doi:10.1103/revmodphys.82.53
2. Hassan AK, Lévy LP, Darie C, Strobel P. Macroscopic Anisotropy and Symmetry Breaking in the Pyrochlore antiferromagnetGd2Ti2O7. *Phys Rev B* (2003) 67(21):214432. doi:10.1103/physrevb.67.214432
3. Lutique S, Staicu D, Konings RJM, Rondinella VV, Somers J, Wiss T. Zirconate Pyrochlore as a Transmutation Target: thermal Behaviour and Radiation Resistance against Fission Fragment Impact. *J Nucl Mater* (2003) 319(none):59–64. doi:10.1016/s0022-3115(03)00134-x
4. Tomasello B, Castelnovo C, Moessner R, Quintanilla J. Single-ion Anisotropy and Magnetic Field Response in the Spin-Ice Materials Ho2Ti2O7 and Dy2Ti2O7. *Phys Rev B* (2015) 92:155120. doi:10.1103/PhysRevB.92.155120
5. Katsufuji T, Hwang HY, Cheong S-W. Anomalous Magnetotransport Properties ofR2Mo2O7near the Magnetic Phase Boundary. *Phys Rev Lett* (2000) 84(9):1998–2001. doi:10.1103/physrevlett.84.1998
6. Shimakawa Y, Kubo Y, Manako T. Giant Magnetoresistance in Ti2Mn2O7 with the Pyrochlore Structure. *Nature* (1996) 379(6560):53–5. doi:10.1038/379053a0
7. Wan X, Turner AM, Vishwanath A, Savrasov SY Topological Semimetal and Fermi-Arc Surface States in the Electronic Structure of Pyrochlore Iridates[J]. *Phys Rev* (2011) 83(20):205101.1–205101.9. doi:10.1103/physrevb.83.205101
8. Prinz GA. Magnetoelectronics. *Science* (1998) 282(5394):1660–3. doi:10.1126/science.282.5394.1660
9. Zutic I, Fabian J, Sarma SD. Spintronics: Fundamentals and Applications[J]. *Rev Mod Phys* (2004) 76(2):323–410. doi:10.1103/RevModphys.76.323
10. Esaki L, Stiles PJ, Molnar Sv. Magnetointernal Field Emission in Junctions of Magnetic Insulators. *Phys Rev Lett* (1967) 19(15):852–4. doi:10.1103/physrevlett.19.852
11. Moodera JS, Hao X, Gibson GA, Meservey R. Electron-Spin Polarization in Tunnel Junctions in Zero Applied Field with Ferromagnetic EuS Barriers. *Phys Rev Lett* (1988) 61(5):637–40. doi:10.1103/physrevlett.61.637
12. Sato K, Bergqvist L, Kudrnovsky J, Dederichs PH, Eriksson O, Turek I, et al. First-principles Theory of Dilute Magnetic Semiconductors[J]. *Rev Mod Phys* (2014) 82(2):1633–90.
13. Tsubokawa I. On the Magnetic Properties of a CrBr3 Single Crystal. *J Phys Soc Jpn* (1960) 15(9):1664–8. doi:10.1143/jpsj.15.1664
14. Dillon JF, Olson CE. Magnetization, Resonance, and Optical Properties of the Ferromagnet CrI3. *J Appl Phys* (1965) 36(3):1259–60. doi:10.1063/1.1714194
15. Mcguire MA, Dixit H, Cooper VR, Sales BC. ChemInform Abstract: Coupling of Crystal Structure and Magnetism in the Layered, Ferromagnetic Insulator CrI_3[J]. *Cheminform* (2015) 46(11):612–20. doi:10.1002/chin.201513017
16. Huang B, Clark G, Navarro-Moratalla E, Klein DR, Cheng R, Seyler KL, et al. Layer-dependent ferromagnetism in a van der Waals crystal down to the monolayer limit. *Nature* (2017) 546(Jun.8):270–3. doi:10.1038/nature22391
17. Gardner JS, Gingras MJP, Greedan JE. Magnetic Pyrochlore Oxides. *Rev Mod Phys* (2010) 82(1):53–107. doi:10.1103/revmodphys.82.53
18. Gajek M, Bibes M, Barthélémy A, Bouzehouane K, Fusil S, Varela M, et al. Spin Filtering through Ferromagnetic BiMnO[J]. *Phys Rev B, Condensed matter* (2005) 72(2):020406. doi:10.1103/physrevb.72.020406
19. Kohn K, Akimoto S-i., Inoue K, Asai K, Horie O. Crystal Structure and Magnetic Properties of MnSeO3, CoSeO3, NiSeO3 and CuSeO3. *J Phys Soc Jpn* (1975) 38(2):587. doi:10.1143/jpsj.38.587
20. Garrett JD, Greedan JE, Maclean DA. Crystal Growth and Magnetic Anisotropy of YTiO3. *Mater Res Bull* (1981) 16(2):145–8. doi:10.1016/0025-5408(81)90074-x
21. Moodera JS, Meservey R, Hao X. Variation of the Electron-Spin Polarization in EuSe Tunnel Junctions from Zero to Near 100% in a Magnetic Field. *Phys Rev Lett* (1993) 70(6):853–6. doi:10.1103/PhysRevLett.70.853
22. Santos TS, Moodera JS. Observation of Spin Filtering with a Ferromagnetic EuO Tunnel Barrier[J]. *Phys Rev B* (2004) 69(69):1681–5. doi:10.1103/physrevb.69.241203
23. Santos TS, Moodera JS, Raman KV, Negusse E, Holroyd J, Dvorak J, et al. Determining Exchange Splitting in a Magnetic Semiconductor by Spin-Filter Tunneling. *Phys Rev Lett* (2008) 101(14):147201. doi:10.1103/physrevlett.101.147201
24. Wachter P. Chapter 19 Europium Chalcogenides: EuO, EuS, EuSe and EuTe. *Handbook Phys Chem Rare Earths* (1979) 2:507–74. doi:10.1016/s0168-1273(79)02010-9
25. Mcguire TR, Shafer MW. Ferromagnetic Europium Compounds. *J Appl Phys* (1964) 35(3):984–8. doi:10.1063/1.1713568
26. Chen W, George J, Varley JB, Rignanese GM, Hautier G. High-throughput Computational Discovery of $In_2Mn_2O_7$ as a High Curie Temperature Ferromagnetic Semiconductor for Spintronics[J]. *npj Comput Mater* (2019) 5(1):1–7. doi:10.1038/s41524-019-0208-x
27. Zhu PW, Jia X, Chen HY, Guo WL, Chen LX, Li DM, et al. A New Method of Synthesis for Thermoelectric Materials: HPHT[J]. *Solid State Commun* (2002) 123(1-2):43–7. doi:10.1016/s0038-1098(02)00182-5
28. Ma S, Bao K, Tao Q, Huang X, Zhu P, Cui T. An Ultra-incompressible Ternary Transition Metal Carbide. *RSC Adv* (2014) 4(108):63544–8. doi:10.1039/c4ra13193b
29. Mao HK, Bell PM. *Carnegie Institution of Washington Year Book*, 77. Washington: Carnegie Institute (1978). p. 904.
30. Hammersley AP, Svensson SO, Hanfland M, Fitch AN, Hausermann D Two-dimensional Detector Software: From Real Detector to Idealised Image or Two-Theta Scan[J]. *High Press Res* (1996) 14(4-6):14. doi:10.1080/08957959608201408
31. Larson AC, Dreele R. *Generalized Structure Analysis System*. Washington, D.C.: GSAS (2000).
32. Birch F. Finite Strain Isotherm and Velocities for Single-crystal and Polycrystalline NaCl at High Pressures and 300°K. *J Geophys Res* (1978) 83:1257–68. doi:10.1029/jb083ib03p01257
33. Scott PR, Midgley A, Musaev O, Muthu DVS, Singh S, Suryanarayanan R, et al. High-pressure Synchrotron X-ray Diffraction Study of the Pyrochlores: Ho2Ti2O7, Y2Ti2O7and Tb2Ti2O7. *High Press Res* (2011) 31(1):219–27. doi:10.1080/08957959.2010.548333
34. Zhang F, Manoun B, Saxena S, Zha CS. Structure Change of Pyrochlore $Sm_2Ti_2O_7$ at High Pressures[J]. *Appl Phys Lett* (2005) 86(18):1906. doi:10.1063/1.1925307
35. Zhao Y, Li N, Xu C, Li Y, Zhu H, Zhu P, et al. Abnormal Pressure-Induced Photoluminescence Enhancement and Phase Decomposition in Pyrochlore La 2 Sn 2 O 7. *Adv Mater* (2017) 29(34):1701513. doi:10.1002/adma.201701513
36. Li H, Li Y, Li N, Zhao Y, Zhu H, Zhu P, et al. A Comparative Study of High Pressure Behaviors of Pyrochlore-type and Thortveitite-type $In_2Ge_2O_7$[J]. *RSC Adv* (2015) 5.
37. Li H, Li N, Zhu P, Wang X. A Comparative Study of High-Pressure Behaviors of the Two Polymorphs of Ho2Ge2O7. *RSC Adv* (2020) 10(18):10540–5. doi:10.1039/c9ra10428c
38. Li H, Ma S, Yu Z, Zhu H, Li N. *In-situ* High-Pressure X-ray Diffraction of the Two Polymorphs of $Sc_2Ge_2O_7$[J]. *AIP Adv* (2020) 10(9). doi:10.1063/5.0021334
39. Zhang S, Li H, Li L, Zhou S. Calculation of Bulk Modulus on Carbon Nitrides with Chemical Bond Method. *Appl Phys Lett* (2007) 91:251905. doi:10.1063/1.2826269
40. Gao F. Hardness Estimation of Complex Oxide Materials. *[J] Phys Rev B* (2004) 69:094113. doi:10.1103/physrevb.69.094113
41. Liu AY, Cohen ML. Prediction of New Compressibility Solids. *J Sci* (1989) 245(4920):841–2. doi:10.1126/science.245.4920.841
42. Zhang FX, Lian J, Becker U, Ewing RC, Hu J, Saxena SK. High-pressure Structural Changes in theGd2Zr2O7pyrochlore. *Phys Rev B* (2007) 76(21):214104. doi:10.1103/physrevb.76.214104
43. Zhang F, Lian J, Becker U, Wang LM, Hu JZ, Saxena S, et al. Structural Distortions and Phase Transformations in $Sm_2Zr_2O_7$ Pyrochlore at High Pressures [J]. *Chem Phys Lett* (2007) 441(4):216–20. doi:10.1016/j.cplett.2007.05.018

Conflict of Interest: The authors declare that the research was conducted in the absence of any commercial or financial relationships that could be construed as a potential conflict of interest.

Publisher's Note: All claims expressed in this article are solely those of the authors and do not necessarily represent those of their affiliated organizations, or those of the publisher, the editors, and the reviewers. Any product that may be evaluated in this article, or claim that may be made by its manufacturer, is not guaranteed or endorsed by the publisher.